Solvation and Solvatochromism in CO_2-Expanded Liquids. 1. Simulations of the Solvent Systems CO_2 + Cyclohexane, Acetonitrile, and Methanol

Hongping Li and Mark Maroncelli*

Department of Chemistry, The Pennsylvania State University, University Park, Pennsylvania 16802

Received: July 3, 2006; In Final Form: August 16, 2006

Molecular dynamics simulations of CO_2-expanded cyclohexane, acetonitrile, and methanol are reported at various compositions along the experimental bubble-point curve at 298 K. Simulated properties include energies, local compositions, viscosities, diffusion coefficients, and dielectric constants and relaxation times. On the basis of the limited comparisons to experimental data currently available, the results indicate that simple intermolecular potential models previously developed for simulating the pure components provide reasonable representations of the energetics and dynamics of these gas-expanded liquids.

I. Introduction

Gas-expanded liquids ("GXLs") are mixtures of a room-temperature organic liquid and a high-pressure gas or supercritical fluid.[1,2] Pressurizing an organic solvent with a gas such as CO_2 near to its critical point can result in substantial incorporation of the gaseous component into the liquid phase. The name gas-expanded liquid refers to the often dramatic (5- to 10-fold) expansion of the original liquid volume that accompanies such gas incorporation.[3] Although the density of GXLs is similar to that of conventional liquids, the presence of the gaseous component leads to solvation and transport properties that are intermediate between those of a dense gas and a conventional liquid. Pressures in the 0−10 MPa range can be used to tune the properties of GXLs, for example their solvent strength, quickly and easily. For this reason, the use of supercritical gases as "antisolvents" for inducing precipitation in micro- and nanoparticle fabrication has proven to be of considerable practical value.[4−6] The enhanced fluidity of GXLs compared to conventional organic solvents also renders them advantageous in separation processes and analytical high-performance liquid chromatography,[7,8] in various cleaning applications,[9] and as reaction media.[2,10−12] Finally, replacement of pure organic solvents with CO_2-expanded liquids is envisioned as a means to decrease the environmental impact and economic cost of common industrial processes.[1,2]

The present paper reports on the first of a series of computational and experimental studies in representative GXLs we have undertaken in order to explore the nature of solvation in this new class of solvents. The experiments include measurements of the solvatochromic shifts of probe solutes, similar to recent work by other groups,[13−16] as well as picosecond and femtosecond measurements of solute rotation and solvation dynamics in GXLs. These experimental data and accompanying computer simulations of solvation in GXLs will be reported in subsequent papers. In this first report we seek to characterize the properties of the model GXLs to be used in the solvation studies. Specifically, we report molecular dynamics simulations of the properties of three CO_2-expanded liquid systems along their experimental bubble point curves at 298 K. The three liquid components, cyclohexane, acetonitrile, and methanol (hereafter referred to as c-C_6H_{12}, CH_3CN, CH_3OH) are chosen to be representative of nonpolar, polar aprotic, and associated solvents. We have calculated a number of energetic, structural, and dynamic properties of these solvent mixtures and, where possible, have compared simulated results to experimental data. Our aim is both to assess the accuracy of simple intermolecular potential models for GXL simulations and to survey the properties of the simulated systems relevant to the forthcoming studies of solvation and solvatochromism. We note that several other workers have recently reported simulations of various aspects of GXL mixtures,[17−23] and we will make comparisons to these studies as we present our results.

II. Models and Simulation Methods

The models use in this study consist of rigid molecules interacting via site−site potentials of the Lennard-Jones (12-6) plus Coulomb type

$$u_{ij}(r_{ij}) = 4\epsilon_{ij}\left\{\left(\frac{\sigma_{ij}}{r_{ij}}\right)^{12} - \left(\frac{\sigma_{ij}}{r_{ij}}\right)^{6}\right\} + \frac{1}{4\pi\epsilon_0}\frac{q_i q_j}{r_{ij}} \qquad (1)$$

where i and j refer to interaction sites on two distinct molecules, r_{ij} is the distance between these sites, ϵ_{ij} and σ_{ij} are the Lennard-Jones parameters, and the q_i values are site charges. The specific models used here were previously parametrized by others in order to reproduce various properties of the neat solvents. Literature references and potential parameters are provided in Table 1. The Lennard-Jones parameters ϵ_i and σ_i in Table 1 refer to interactions between identical sites ($i \leftrightarrow ii$). Parameters for distinct site interactions are obtained from the former parameters using the combining rules $\epsilon_{ij} = (\epsilon_{ii}\epsilon_{jj})^{1/2}$ and $\sigma_{ij} = (1/2)(\sigma_{ii} + \sigma_{jj})$.

Simulations were performed using a modified version of the DL_POLY program.[24] Neat solvent systems consisted of 343 (c-C_6H_{12}), 512 (CH_3CN, CH_3OH), or 1000 (CO_2) molecules. All GXL mixtures consisted of a total of 1000 molecules. The simulations reported here were performed in the NVT ensemble at a temperature of 298 K using a Nose-Hoover thermostat.[25] For convenience, dynamical as well as equilibrium quantities were calculated in the NVT ensemble. Tests using the NVE ensemble showed that any perturbation of the dynamics caused by the thermostat was smaller than the uncertainties in the data

* Corresponding author: maroncelli@psu.edu.

10.1021/jp064166j CCC: $33.50
Published on Web 09/29/2006

TABLE 1: Simulation Models[a]

molecule	site	ϵ_i/kJ mol^{-1}	σ_i/Å	q_i/e	geometry	ref	V_{vdW}/Å^3	μ/D	$\langle Q \rangle$/DÅ
CO_2	C	0.2339	2.757	0.6512	$l = 1.149$ Å	39	29.2	0	4.13
	O	0.6694	3.033	−0.3256					
c-C_6H_{12}	CH_2	0.4937	3.905	0	$l = 1.530$ Å, $\theta = 112°$	40	104.8	0	0
CH_3CN	CH_3	1.588	3.6	0.269	$l(CH_3-C) = 1.46$ Å,	41	44.8	4.12	0.98
	C	0.4157	3.4	0.129	$l(CN) = 1.17$ Å				
	N	0.4157	3.3	−0.398					
CH_3OH	CH_3	0.7579	3.861	0.297	$l(CH_3-O) = 1.425$ Å,	42	36.6	2.33	1.39
	O	0.7312	3.083	−0.728	$l(O-H) = 0.945$ Å,				
	H	0	0.000	0.431	$\theta = 108.53°$				

[a] V_{vdW} is the volume bounded by the Lennard-Jones radii ($\sigma_i/2$) of the sites comprising the molecule, μ is the dipole moment, and $\langle Q \rangle$ the effective quadrupole moment, $Q^2 = (2/3)\mathrm{Tr}[\mathrm{Q:Q}]$[43] of the model charge distribution.

TABLE 2: Effective Pair Interaction Energies (298 K)[a]

system	$-e_{11}$/kJ mol^{-1}	$-e_{12}$/kJ mol^{-1}	$\Delta e/k_BT$	$-g_{11}$/kJ mol^{-1}	$-g_{12}$/kJ mol^{-1}	$\Delta g/k_BT$
$CO_2 + CO_2$	2.8			1.6		
c-$C_6H_{12} + CO_2$	6.4	3.7	0.7	4.0	2.6	0.2
$CH_3CN + CO_2$	16.1	5.9	2.9	9.7	3.1	2.1
$CH_3OH + CO_2$	23.7	6.2	5.7	10.3	2.3	2.9
c-$C_6H_{12} + CH_3CN$			5.2			2.7
c-$C_6H_{12} + CH_3OH$			9.6			3.9

[a] The subscripts "1" and "2" here denote the first and second components of each system as written.

of interest. Cubic periodic boundary conditions were applied and long-range interactions treated using the standard Ewald method. Rigid body equations of motion employing a quaternion representation of rotational degrees of freedom were integrated using a leapfrog scheme with a 2 fs time step. After 0.5−1 ns equilibration from a lattice configuration, simulations were run for between 1 and 2 ns for data collection. Trajectory data were typically collected in 100−200 ps blocks, and the blocks were averaged in order to obtain estimates of statistical uncertainties (standard errors of the mean) for the results reported.

III. Structure and Energetics

Before discussion of the simulation results, it is useful to consider the characteristics of the molecules constituting these mixtures and the interactions among them. Table 1 lists the van der Waals volumes and the first two electrostatic moments of the model molecules. As is typical of GXLs, the liquid component molecules are larger than those of the gaseous CO_2 component. The polar liquids CH_3OH and CH_3CN are actually atypically small compared to most liquid solvents, yet they still have van der Waals volumes that are ∼30% and 50% larger than that of CO_2. The nonpolar liquid c-C_6H_{12} is more typical in that it consists of molecules that are more than three times larger than CO_2.

Differences in the electrostatic characteristics of the constituent molecules give rise to significantly different interaction energies. Table 2 provides some measure of these energies in terms of the depths of effective molecular pair potentials. The e_{ij} values listed in Table 2 are the minimum values of orientationally averaged pair interaction energies

$$e_{ij} = \min \langle V_{ij}(R_{ij},\vec{\Omega}_{ij}) \mathrm{e}^{-V_{ij}/k_BT} \rangle_{\vec{\Omega}_{ij}} \qquad (2)$$

and the g_{ij} are corresponding minima in the free energies

$$g_{ij} = \min\{-k_BT \ln \langle \exp\{-V_{ij}(R_{ij},\vec{\Omega}_{ij})/k_BT\} \rangle_{\vec{\Omega}_{ij}}\} \qquad (3)$$

where V_{ij} is interaction potential between two molecules separated by a center of mass distance R_{ij} and having a relative orientation $\vec{\Omega}_{ij}$.[26] The energy mismatches

$$\Delta e = 2e_{12} - e_{11} - e_{22}, \qquad \Delta g = 2g_{12} - g_{11} - g_{22} \qquad (4)$$

relative to the thermal energy k_BT provide indicators of the extent of nonideality expected for a given mixture. Simple models[27,28] predict that values of $\Delta e/k_BT$ or $\Delta g/k_BT$ greater than a certain threshold value (∼0.5) signal incomplete miscibility. For calibration purposes we have included in Table 2 values of these quantities calculated for the immiscible liquid−liquid mixtures c-C_6H_{12} + CH_3CN and c-C_6H_{12} + CH_3OH. These comparisons indicate that c-C_6H_{12} should form more nearly ideal mixtures with CO_2 than should the liquids CH_3CN and CH_3OH. The energetic disparity between the CO_2 interactions with these polar liquids is comparable to that between them and the nonpolar liquid c-C_6H_{12}.

We now consider the simulated energetic and structural properties of the GXLs summarized in Table 3. The first three columns of Table 3 reproduce some experimentally determined properties of the GXLs in coexistence with their vapor phases (nearly pure CO_2) at 298 K. These are conditions we have used in spectroscopic measurements to be described in forthcoming work[29] and these are the conditions to be modeled by simulation. Rather than determining the coexistence properties of the model GXLs in order to simulate along the *model* coexistence curves, we have instead performed constant (N, V, T, x) simulations at the liquid-phase densities determined experimentally. We do so in order to facilitate direct comparison to experiment without the need to tune potential parameters. Prior work on CO_2-expanded CH_3CN,[21] CH_3OH,[18,20,22] and similar GXLs[22] has shown that potentials of the sort employed here provide fairly accurate representations of the bubble-point curve, even without adjustment. In the present case, errors in the model potentials cause the pressures of the simulated systems to differ from the experimental pressures, in some cases by as much as 50 MPa at small mole fractions of CO_2. But, as will be shown below, such inaccuracies do not prevent the models from yielding good agreement with experiment for a number of properties of the GXLs.

Figure 1 highlights one aspect of the data in Table 3 which provides useful perspective on the nature of these mixtures. The appellation "gas-expanded liquid" tends to connote solvents that are somehow rarefied compared to conventional liquid solvents. In what sense is this notion correct? The top panel of Figure 1 shows that the mass density in these prototypical GXLs actually increases over much of the composition range commonly explored in experiment. All three liquids exhibit a density maximum that is 10−15% higher than the density of the pure liquid component. This increased density persists up to $x_2 = 0.9$, where the original liquid volume is expanded approximately 10-fold, and it is only at very high x_2 that the GXL density

TABLE 3: Energetic and Structural Properties

x_2	P/MPa	V/cm^3 mol^{-1}	f_{occ}	$-E_{conf}$/kJ mol^{-1}	f_{el}	δ/(MPa)$^{1/2}$	$N(1)$	$N(2)$	$x_2(1)$	$x_2(2)$
				c-C_6H_{12}(1) + CO_2(2)						
0.000	0.1	108.7	0.58	31.5	0.00	17.0	8.9			
0.100	0.8	101.7	0.58	29.4	0.00	17.0	9.4	8.7	0.093	0.096
0.400	3.2	81.6	0.55	23.0	0.01	16.8	11.0	10.6	0.381	0.404
0.700	4.9	64.3	0.49	16.2	0.05	15.9	13.0	13.0	0.683	0.707
0.800	5.2	59.6	0.45	13.8	0.08	15.2	13.7	13.9	0.788	0.805
0.950	5.9	56.2	0.35	9.8	0.15	13.2	14.3	14.5	0.943	0.951
				CH_3CN(1) + CO_2(2)						
0.000	0.1	52.9	0.51	34.1	0.47	25.4	10.1			
0.262	1.6	50.7	0.48	27.7	0.45	23.4	10.4	10.2	0.256	0.266
0.461	3.1	48.8	0.46	23.0	0.41	21.7	10.7	10.5	0.445	0.470
0.660	4.5	48.0	0.43	18.1	0.36	19.4	10.9	10.6	0.621	0.672
0.840	5.2	48.9	0.39	13.4	0.29	16.5	10.8	10.5	0.779	0.846
0.864	5.3	49.4	0.38	12.7	0.28	16.0	10.8	10.4	0.805	0.868
0.950	6.0	54.4	0.33	9.8	0.22	13.4	10.2	9.5	0.895	0.950
				CH_3OH(1) + CO_2(2)						
0.000	0.1	40.7	0.54	35.2	0.84	29.4	12.7			
0.229	3.0	41.4	0.51	29.4	0.77	26.6	12.4	12.2	0.216	0.259
0.420	4.9	42.8	0.47	24.2	0.70	23.8	12.1	11.7	0.368	0.477
0.629	5.7	45.7	0.42	18.4	0.59	20.0	11.5	11.0	0.503	0.688
0.811	5.9	49.2	0.37	13.4	0.44	16.5	11.0	10.3	0.624	0.844
0.969	6.2	56.8	0.31	8.8	0.22	12.5	9.7	9.2	0.869	0.971

Neat CO_2

x_2	P/MPa	V/cm^3 mol^{-1}		$-E_{cnf}$/kJ mol^{-1}	f_{el}	δ/(MPa)$^{1/2}$	$N_{6Å}$	$N_{7Å}$
1.000	6.5	61.5	0.29	7.8	0.18	11.3	8.6	13.4
1.000	20	48.1	0.37	9.8	0.18	14.3	10.6	16.7

[a] Values of the mole fraction, x_2, pressure, P, and molar volume, V, correspond to those of the experimental systems. In the case of c-C_6H_{12} + CO_2 these values are estimated from the Peng−Robinson equation of state.[44] Values for CH_3CN + CO_2, CH_3OH + CO_2, and neat CO_2 are from the experimental data in refs 45−47. (The data for the $x_2 = 0.95$ composition of CH_3CN + CO_2 are an extrapolation.) f_{occ} is the packing fraction or fractional volume occupied by molecules obtained by using the van der Waals volumes in Table 1 for molecular volumes. E_{conf} is the configurational energy of the system and f_{el} is the fraction of this energy contributed by electrostatic interactions. δ is the Hildebrand solubility parameter, here given by $\delta = (-E_{conf}/V)^{1/2}$. $N(1)$ and $N(2)$ are the coordination numbers of components 1 and 2 and $x_2(1)$ and $x_2(2)$ are the local mole fractions in the first coordination shells of components 1 and 2 (see text). The statistical uncertainty in all of these quantities is typically on the order of 1% or less.

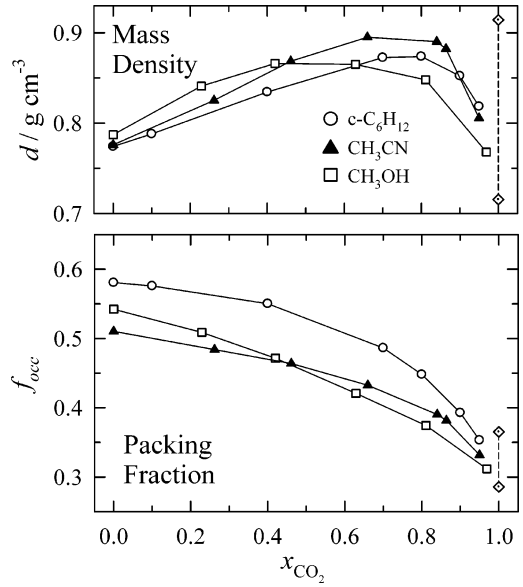

Figure 1. Volumetric properties of the GXLs studied. The top panel shows the mass densities and the bottom panel the packing fractions, the ratios of the volumes occupied by molecules to the molar volumes. In both panels the two diamonds connected by a dashed line indicate the values of these quantities in pure CO_2 at 298 K and at pressures of 6.5 (lower) and 20 MPa (upper point).

actually drops below that of the original liquid. Thus, GXLs cannot be considered to be rarified in the sense that they have larger molar volumes (Table 3) or lower mass densities than conventional liquid solvents. The sense in which they are rarified is shown in the bottom panel of Figure 1. Here we have plotted the packing fraction, the fraction of the total volume of the system that is occupied by the van der Waals volumes of the constituent molecules. In all three liquids this packing fraction decreases monotonically to values of ∼60% of those found in the original liquids at high CO_2 dilutions. Although we use the van der Waals volumes defined by the Lennard-Jones parameters of the simulation models here, the same conclusion is reached using other estimates of molecular volumes. Thus, these liquids are rarified in the sense that there is considerably more "free-volume" present in the GXL than in the original liquids. This extra space is likely to be the primary source of the enhanced solubilities of gases and the enhanced fluidity of GXLs compared to conventional liquid solvents. At least in the case of CO_2 as the expanding gas, this extra free volume results from the fact that CO_2 molecules are smaller than those of the liquid components studied.

Figure 2 shows how the configurational energies, the net potential energy resulting from intermolecular interactions, vary as functions of composition. The negatives of these energies are the simulated values of the vaporization energies ($\Delta_{vap}U$) and represent the cohesive energies binding the GXL molecules together. The models used here do a reasonable job of reproducing the binding energies of the neat component liquids. With the exception of CH_3CN, where the simulation overestimates $\Delta_{vap}U$ by 11%, the energies calculated for c-C_6H_{12}, CH_3OH, and CO_2 are all within 1−4% of the experimental values. The configurational energies are nearly linear functions of composition along the bubble-point curve. With the 6.5 MPa

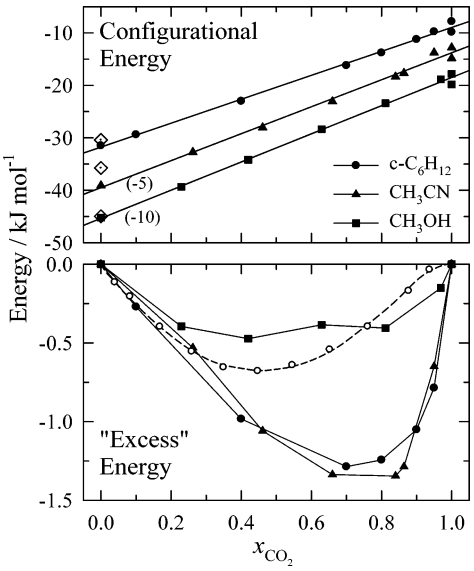

Figure 2. Configurational energies as functions of composition. The top panel shows the simulated configurational energies directly (filled symbols). The larger diamonds at $x = 0$ are experimental values of the energy of vaporization of the neat liquids.[31] Two simulated points for neat CO_2 at 6.5 and 20 MPa are also shown. For clarity, data corresponding to the $CH_3CN + CO_2$ and $CH_3OH + CO_2$ systems have been shifted by −5 and −10 kJ/mol, respectively. The bottom panel shows "excess" configurational energies using the neat organic liquids and neat CO_2 ($P = 6.5$ MPa) as reference points (eq 5). The filled symbols are simulated values, and the open symbols and dashed curve show the excess enthalpies measured at a 298 K and a fixed pressure of 7.5 MPa[30] for the $CH_3OH + CO_2$ system.

neat CO_2 point for the CO_2 reference ($E_2°$), "excess" energies calculated according to

$$E^{ex} = E_{conf}(x_2) - \{(1 - x_2)E_1° + x_2E_2°\} \qquad (5)$$

are displayed in the bottom panel of Figure 2. These data are not proper excess quantities in that they do not correspond to a fixed pressure. Nevertheless, they are useful for gauging the energetic nonideality of the mixtures. The closest experimental comparison available to these pseudo excess energies is to excess enthalpy data for $CH_3OH + CO_2$ measured at 298 K and 7.5 MPa.[30] The fact that these data, also shown in Figure 2, are in semiquantitative agreement with the simulated values suggests that the model energies are reasonable over the entire composition range. It is interesting that the excess energies calculated for the CH_3OH system are much smaller than those for the c-C_6H_{12} and CH_3CN systems. This is not what one would anticipate from the pairwise excess energies listed in Table 2.

The relative contributions made by electrostatic interactions to the configurational energies are also listed in Table 3. In neat CO_2 the fraction of the energy that is electrostatic in origin is estimated to be about 18%. In neat c-C_6H_{12} this fraction is zero (the site charges are all zero in the simulation model), and in the c-$C_6H_{12} + CO_2$ mixture electrostatic interactions are never of much importance. In the CH_3CN system the electrostatic and Lennard-Jones components of the interactions are of comparable magnitude whereas in CH_3OH, due to the strength of hydrogen bonding interactions, they dominate at low x_{CO_2}. These differences underscore the broad range of behavior reflected in the three GXLs chosen for study. The range of values of the Hildebrand solubility parameters spanned by these systems (Table 3) also reflects this breadth of character. For example, approximately 95% of all common liquid solvents have solubility parameters between those of c-C_6H_{12} (16.8 $MPa^{1/2}$) and CH_3OH (29.3 $MPa^{1/2}$).[31]

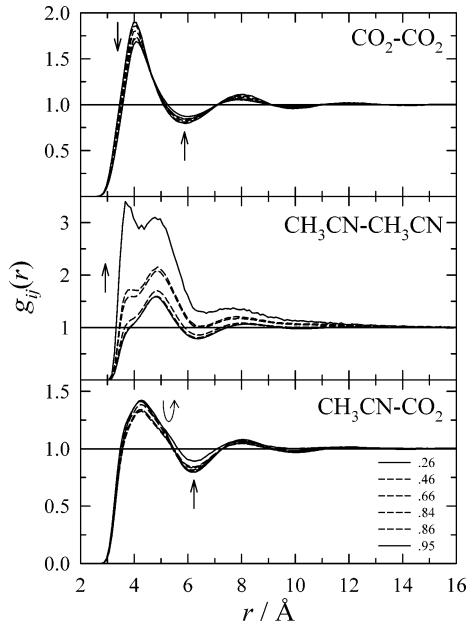

Figure 3. Center-of-mass radial distribution functions of $CH_3CN + CO_2$. The two limiting compositions (x_{CO_2}) are shown as solid lines and the intermediate ones as dashed lines. Arrows indicate the direction of increasing x_{CO_2}.

We now briefly examine the structure present in these mixtures. For simplicity we mainly consider radial distribution functions of the center-of-mass separations of the molecules involved. Such distributions for the $CH_3CN + CO_2$ case are shown in Figure 3. In the $CH_3CN + CO_2$ system, as well as in the other two GXLs, there is little qualitative change in the CO_2-CO_2 distribution ($g_{22}(r)$) with composition. The main change with increasing x_{CO_2} is a tendency for $g_{22}(r)$ to approach unity—i.e., a modest decrease in the overall order of the liquid as reported by the CO_2-CO_2 distribution. Similar behavior was noted in simulations of acetone + CO_2 and $CH_3OH + CO_2$ by Shulka et al.[23] The $CH_3CN + CO_2$ distribution $g_{12}(r)$ shows a more complicated behavior. The peak of this function first decreases with increasing x_{CO_2} and then increases at sufficiently high CO_2 concentrations ($x_{CO_2} > 0.9$). The same nonmonatonic dependence is also observed in the two other GXLs. But these changes are also relatively modest. The only marked changes with composition are found in the liquid component distributions, $g_{11}(r)$. This distribution for $CH_3CN + CO_2$ is shown in the middle panel of Figure 3, and the corresponding functions for the two other GXLs are shown in Figure 4. In the c-C_6H_{12} + CO_2 mixture, the main effect of added CO_2 is a blurring of the initially well-defined long-range structure present in the neat c-C_6H_{12} liquid. But in the two polar systems CH_3CN and CH_3OH there is a pronounced growth in the first peak of g_{11} at high CO_2 concentrations. This growth reflects the preferential association of the liquid component molecules with one another. In the case of CH_3CN, there is a 2-fold increase in the maximum of g_{11}, and also a change in the relative heights of the two components of first the peak. Atom−atom distribution functions (see Figure S1 in Supporting Information) suggest that this change in shape reflects a greater prevalence of antiparallel pairs of CH_3CN molecules at high dilution, as recently proposed by Houndonougbo et al.[21] based on more detailed analyses. In the methanol case, the g_{11} maximum increases dramatically, to values greater than 20 at the highest dilution, a result of the persistence of many CH_3OH-CH_3OH hydrogen bonds even at

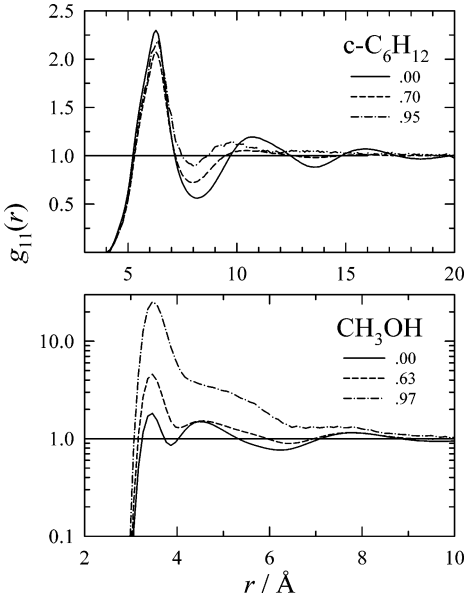

Figure 4. Center-of-mass radial distribution functions g_{11} of the liquid components of c-C_6H_{12} + CO_2 and CH_3OH + CO_2.

high x_{CO_2}. Two groups have recently analyzed the composition dependence of hydrogen bonding in comparable models of CH_3OH + CO_2 in some detail.[18,20] Here we only make the crude observation that, based on H−O distribution functions (Figure S2), more than half of the H(O) atoms of CH_3OH remain hydrogen bonded up to CO_2 mole fractions as high as 0.9.

Finally, we quantify the extent of the preferential association noted above by integrating the center-of-mass distribution functions out to distances R_1 approximately encompassing the first solvation shell of each species. The results are summarized in the last four columns of Table 3. For each GXL we use a composition- and species-independent value of the radius R_1. In the case of the CH_3CN and CH_3OH mixtures we choose R_1 = 6 Å and in the case of c-C_6H_{12} + CO_2 we use R_1 = 7 Å. $N(1)$ and $N(2)$ in Table 3 denote net coordination numbers, i.e., the total numbers of molecules within R_1 of components 1 (liquid) and 2 (CO_2), and $x_2(1)$ and $x_2(2)$ denote the local CO_2 mole fractions in these regions. By virtue of the similar size and shape of CH_3CN and CO_2 molecules, the coordination numbers defined in this manner are nearly constant at the value 10.5 in the CH_3CN + CO_2 mixture. In the other two systems, the coordination numbers vary over wider ranges, averaging 11.9 in the c-C_6H_{12} + CO_2 system and 11.2 in c-CH_3OH + CO_2. Although these numbers vary with choice of R_1, the local compositions $x_2(i)$ are not very sensitive to this choice as long as the integration captures most of the first peak of the distributions.

In Figure 5 the 1(1) "enrichment" factors, defined as the ratio of the local mole fraction of component 1 (the liquid component) in the first solvation shell of a molecule of 1 relative to the bulk mole fraction of 1. (Enrichment factors for other components can be readily derived from the data in Table 3; they are all much closer to unity than the values depicted.) Figure 5 shows that there is little solvent sorting in the c-C_6H_{12} + CO_2 GXL at any CO_2 concentration. In contrast, for mole fractions of CO_2 greater than 0.5, the polar solvents CH_3CN and CH_3OH show a significant preference for self-association. At x_{CO_2} ~ 0.95, one finds twice as many CH_3CN molecules in the first solvation shell of a central CH_3CN molecule than expected for random mixing. In the case of the CH_3OH mixture this preference amounts to more than a factor of 4. In both of these latter cases, visual inspection of simulated configurations show obvious clusters of component 1 molecules at high dilution in CO_2 whereas an approximately random distribution is always observed in the c-C_6H_{12} + CO_2 mixture.

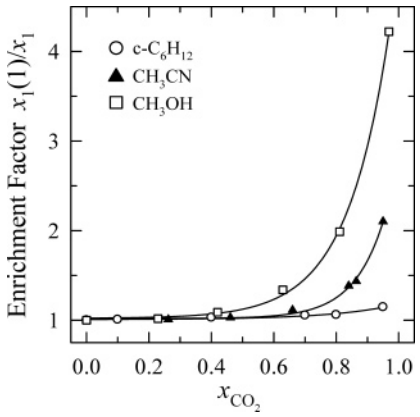

Figure 5. Component 1 enrichment factors $x_1(1)/x_1$ versus CO_2 mole fraction (x_2). The curves shown here are fits to functions of the form $x_1(1)/x_1 = 1 + a \exp(-bx_2)$.

TABLE 4: Dynamical and Dielectric Properties[a]

x_2	η/cP	$D_1/10^{-9}$ m s^{-1}	$D_2/10^{-9}$ m^2 s^{-1}	ϵ_r/kJ mol^{-1}	τ_M/ps
		c-$C_6H_{12}(1)$ + $CO_2(2)$			
expt[b]	0.90	1.4		2.0	
0.000	0.55	2.47		(1)	
0.100	0.46	2.79	6.23	(1)	
0.400	0.28	3.44	7.20	(1)	
0.700	0.22	5.25	9.74	(1)	
0.800	0.13	6.30	11.35	(1)	
0.950	0.10	10.90	16.81	(1)	
		$CH_3CN(1)$ + $CO_2(2)$			
expt[b]	0.34	4.9		35.8	3.4
0.000	0.33	3.34		29.0	3.8
0.262	0.29	4.40	6.49	20.7	3.4
0.461	0.22	5.18	7.30	15.0	3.4
0.660	0.15	6.34	9.56	9.3	3.1
0.840	0.10	7.90	12.33	4.2	2.3
0.864	0.091	8.76	13.26	3.6	2.3
0.950	0.080	12.56	17.25	1.8	1.7
		$CH_3OH(1)$ + $CO_2(2)$			
expt[b]	0.55	2.3		32.5	46
0.000	0.54	2.08		18.7	21
0.229	0.34	2.91	5.80	14.2	17
0.420	0.25	3.97	7.72	10.1	17
0.629	0.16	5.60	10.91	5.4	11
0.811	0.095	7.74	14.05	2.7	6.6
0.969	0.067	13.55	20.01	1.2	0.7
		Neat CO_2			
expt 6.5 MPa[c]	0.058		24.7	1.43	
expt 20 MPa[c]	0.095		15.5	1.57	
6.5 MPa	0.079		22.90	(1)	
20 MPa	0.105		14.19	(1)	

[a] Estimated uncertainties in the simulated values listed are as follows: viscosity η, ±10−20%; diffusion constants D_1 and D_2, ±5%; relative permittivity ϵ_r, <±7%; and dielectric relaxation times τ_M, <±10% for CH_3CN and <±20% for CH_3OH mixtures. [b] Liquid solvent values of η and D are from tabulated data in ref 31 and ϵ_r and τ_M values are from refs 48 and 49. [c] CO_2 values of η are from ref 47 and D and ϵ_r values from the parametrizations in refs 50 and 51.

IV. Dynamical & Dielectric Properties

To characterize dynamics in these GXLs, we have calculated the properties listed in Table 4. Shear viscosities η were calculated by integrating the autocorrelation function of the stress tensor

$$\eta = \frac{V}{k_B T}\int_0^\infty \mathrm{d}t\langle P_{\alpha\beta}(0)P_{\alpha\beta}(t)\rangle \quad (6)$$

where α and β denote distinct Cartesian coordinates.[32,33] Simulated viscosities are plotted in Figure 6 together with some comparisons available from experiment. Viscosities of the neat liquids are readily available, and they are listed in Table 4. With the exception of c-C_6H_{12}, the models reproduce the pure solvent viscosities to within the estimated uncertainties in the simulated values (10−20%). In contrast, the viscosity of neat c-C_6H_{12} is poorly reproduced using the present model and is lower than the experimental value by almost 40%. Unfortunately, there are few direct measurements of viscosities in GXLs. The only data available on the present systems are the chromatographic measurements of Cui and Olesik[7] on $CH_3OH + CO_2$ at 298 K and 17.2 MPa. These data are shown plotted as the small open triangles and dashed curve in the bottom panel of Figure 6. The experimental data are uniformly higher than the simulated values, by between 10% ($x_2 = 0$) and 50% ($x_2 = 1$). Such a difference is approximately what would be expected to result from the pressure differentials between the experiment and simulations. This comparison therefore suggests that the present models probably provide a faithful representation of the viscosity of $CH_3OH + CO_2$ along the coexistence curve. In the case of the two other GXLs, we have plotted viscosities estimated from solute rotation times for comparison to the simulated data. These estimates are based on fluorescence anisotropy measurements of the probe 9,10-bis(phenylethynyl)anthracene (PEA) similar to those described in ref 34. To produce the estimates in Figure 6, we employed the empirical correlation

$$\ln\left(\frac{\eta/\mathrm{cP}}{T/\mathrm{K}}\right) = -15.040 + 2.630\ln(\tau_{rot}/\mathrm{ps}) - 0.152\{\ln(\tau_{rot}/\mathrm{ps})\}^2 \quad (7)$$

developed from the liquid and neat CO_2 data reported in ref 34. This relationship fits available data over the viscosity range ($0.02 < \eta < 3$ cP; $T \sim 300$ K) with a standard error of 0.14. In the case of c-$C_6H_{12} + CO_2$ the agreement between these experimental estimates of viscosity and the simulated values is poor. In $CH_3CN + CO_2$ the two agree to within uncertainties. It is interesting that the experimental data indicate a nearly linear dependence of η upon x_{CO_2} in the case of $CH_3CN + CO_2$ but a clearly nonlinear dependence in $CH_3OH + CO_2$. The simulations nicely reproduce this distinction.

The self-diffusion coefficients listed in Table 4 were calculated from the slopes of the atomic displacements $\vec{r}_i$ via the Einstein relation

$$D_i = \lim_{t\to\infty}\frac{1}{6}\frac{d\langle|\vec{r}_i(t) - \vec{r}_i(0)|^2\rangle}{dt} \quad (8)$$

These data are plotted as functions of composition in Figure 7. The only experimental data for comparison are at the pure component limits (large diamonds in Figure 7) where we find errors in the simulated values of −8% in CO_2, +75% in c-C_6H_{12}, −31% in CH_3CN, and −10% in CH_3OH. With the exception of c-C_6H_{12}, where the viscosity is also poorly modeled, this level of agreement is satisfactory. Between the pure solvent limits the simulated diffusion coefficients are highly nonlinear functions of x. The present results for $D(CH_3OH)$ in $CH_3OH + CO_2$ are fairly close to those calculated by Shulka et al. using different CH_3OH and CO_2 potentials.[23] If the diffusion follows simple Stokes−Einstein hydrodynamic behavior, one would expect the products ηD_i to be constant for each species i, with the values of ηD_i varying according to the inverse of the effective radius of i. Although the uncertainties in the simulated data are sizable, it is clear that these products are far from constant (Figure S3). The simulated values of ηD_i decrease for

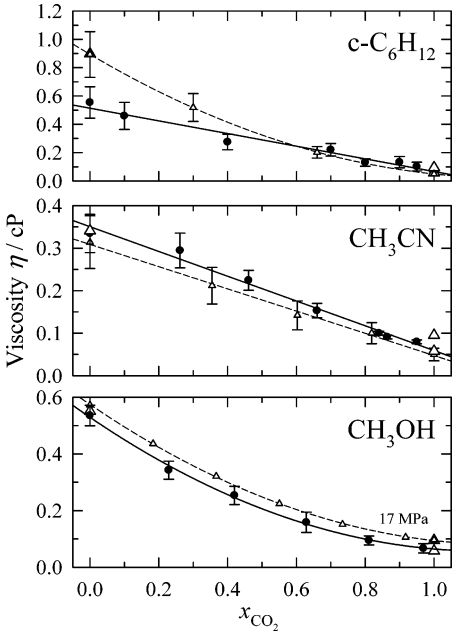

Figure 6. Comparison of simulated viscosities (filled symbols and solid curves) and experimental estimates (open symbols and dashed curves). In the CH_3OH case the experimental data are actual viscosity measurements made at a higher, constant pressure of 17.2 MPa.[7] In the other two systems the experimental data are estimated from rotation times as described in the text. The simulated and experimental data here are fit to $\eta/\mathrm{cP} = a_0 + a_1x + a_2x^2$ with the following parameters (a_0, a_1, a_2): c-C_6H_{12}, sim = (0.51, −0.44,0), expt = (0.89, −1.43,0.59); CH_3CN, sim = (0.35, −0.29,0), expt = (0.31, −0.26); CH_3OH, sim = (0.53, −0.83,0.36), expt = (0.57, −0.82,0.34).

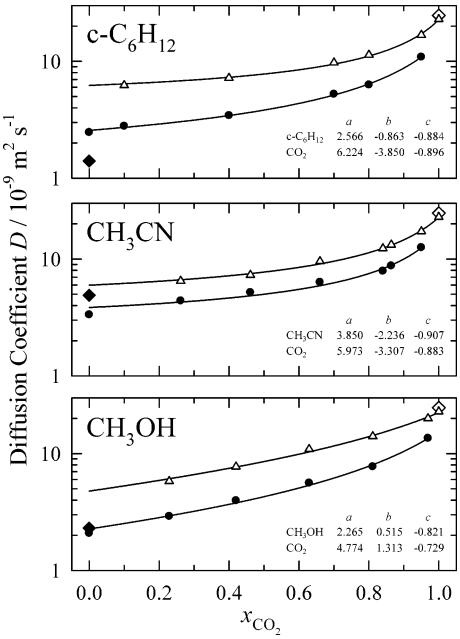

Figure 7. Simulated self-diffusion coefficients of CO_2 (open symbols) and the liquid component (filled symbols) of the GXLs. The large symbols at the $x = 0$, 1 limits are experimental values.[31,47] The curves are fits to the functional form $D/(10^{-9}\ \mathrm{m^2\ s^{-1}}) = (a + bx)/(1 + cx)$ with the parameters shown on the inset to each panel.

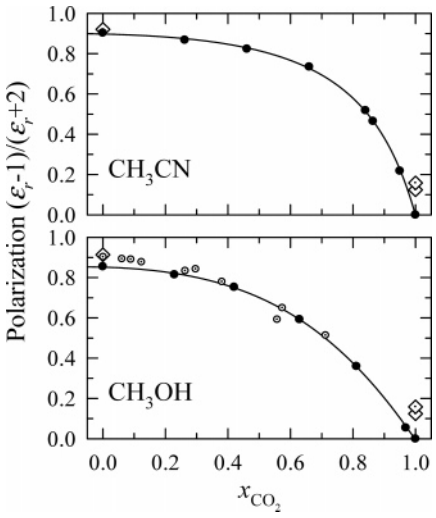

Figure 8. Permittivity or reaction field factor $(\epsilon_r - 1)/(\epsilon_r + 2)$ vs x. Filled symbols denote simulation results and open symbols experimental data. The experimental data on the $CH_3OH + CO_2$ mixture (small triangles) are for $T = 323$ K and $P = 11$ MPa, from refs 19 and 38. The curves are fits of the simulation data to $f(\epsilon_r) = (a + bx)/(a + cx + dx^2)$ with the constants $(a, b, c, d) = (0.898, -0.898, -0.959, 1.192)$ in the CH_3CN mixtures and $(0.852, -0.854, -0.953, 0.330)$ in the CH_3OH mixtures.

all species, by about 30% for the liquid component molecules and by an average of 45% for CO_2.

The final aspect of these mixtures we have examined is their dielectric properties, both static and dynamic. The relative permittivities in Table 3 were calculated using the relation[32]

$$\epsilon_r = 1 + \frac{4\pi\langle|\vec{M}|^2\rangle}{3k_B TV} \tag{9}$$

where $\vec{M}$ denotes the net dipole moment of the simulation cell. The dielectric relaxation times τ_M listed here are the $1/e$ times of the decay of the autocorrelation function of $\vec{M}$

$$\Phi_M(t) = \langle\vec{M}(0)\cdot\vec{M}(t)/\langle|\vec{M}|^2\rangle\rangle \tag{10}$$

In the absence of explicit electronic polarizability, dielectric properties can only be obtained for the dipolar species CH_3CN and CH_3OH and their mixtures with CO_2. In the case of neat CH_3CN, the simulation models reproduce both experimental values of ϵ_r and τ_M to better than 20%. For neat CH_3OH the situation is less satisfying. Here ϵ_r is lower than the experimental value by 43% and, more importantly, the dielectric time τ_M is too small by more than a factor of 2. This latter feature of the H1 model of CH_3OH used here has been noted previously[35] and apparently is a failing common to other simple models of methanol.[36]

The dependence of solvent polarity upon composition is illustrated in Figure 8. Rather than plotting the permittivity directly, we plot the polarization or reaction field factor

$$f(\epsilon_r) = \frac{\epsilon_r - 1}{\epsilon_r + 2} \tag{11}$$

This factor is used here because it (or a close variant) is what is commonly used to relate solvation energies of dipolar species to solvent permittivity and is thus more relevant to the problems of solvatochromism that we are ultimately interested in. In contrast to ϵ_r itself, which is a surprisingly linear function of x in the case of the $CH_3CN + CO_2$ mixture, $f(\epsilon_r)$ is a strongly

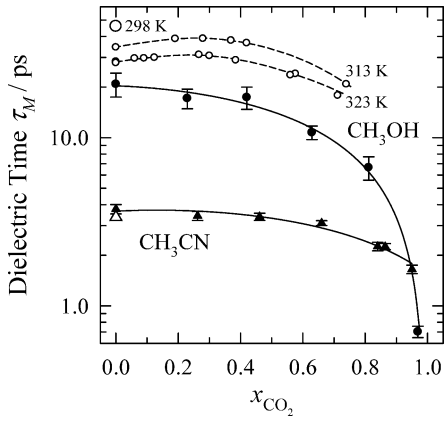

Figure 9. Composition dependence of dielectric relaxation times, t_{1e} of $\Phi_M(t)$. Filled symbols are simulation results and open symbols experimental data. The experimental data of Smith et al.[38] at 11 MPa and two temperatures 313 and 323 K are shown as the small open circles.

nonlinear function in both GXLs. This "dielectric nonideality"[37] implies that solvation energies and spectral shifts will be nonlinear functions of composition in these mixtures, even in the absence of preferential solvation of the solute. It should also be noted from Figure 8 that the large relative error in ϵ_r made by the model in the neat CH_3OH case is greatly reduced when considering $f(\epsilon_r)$ and thus solvation energies. Figure 8 also includes experimental results for the concentration dependence of $f(\epsilon_r)$ in $CH_3OH + CO_2$ from the data of Smith et al.,[19,38] which are denoted by the smaller open symbols. These experimental data were recorded in the single-phase region at 323 K and 11 MPa and so do not correspond exactly to the simulation conditions. Nevertheless, the similarity of the x-dependences in the two sets of data suggests that the polarity of the $CH_3OH + CO_2$ mixture is realistically modeled in these simulations. It is not unreasonable to expect that the same is true in the $CH_3CN + CO_2$ case.

The composition dependence of the dielectric relaxation times in these mixtures is plotted in Figure 9. We note that $\Phi_M(t)$ can be reasonably represented by single-exponential functions of time in the $CH_3CN + CO_2$ mixtures. In contrast, triple exponential functions are required for adequate fits of the $CH_3OH + CO_2$ data. (See Figures S4 and S5.) Because of this complexity, the $1/e$ times in Figure 9 is only a partial characterization of the dielectric response in the latter case. As illustrated here, upon dilution with CO_2 these times decrease substantially—by a factor of 2 in the case of CH_3CN and by a much larger factor in CH_3OH. In the CH_3OH case the precipitous drop in τ_M is undoubtedly related to the breakup of the larger CH_3OH aggregates responsible for the slow relaxation characteristic of normal alcohols. The experimental results of Smith et al.[19,38] (11 MPa, 313 and 323 K) for the $CH_3OH + CO_2$ mixture are also plotted in Figure 9 (small open symbols). Despite the higher temperatures of the experimental data, the simulated times are all smaller than the experimental times. Whatever shortcomings of the CH_3OH model cause its dielectric relaxation to be much too fast in neat CH_3OH apparently carry over into the mixtures. As in the case of neat CH_3OH,[35] this discrepancy is likely to render solvation dynamics predicted using these models significantly faster than what is measured in experiment. It is not possible to decide from the available data the extent to which the simulated composition dependence of τ_M is accurate. Neither of the simulated systems show the subtle maximum in τ_M exhibited by the experimental $CH_3OH + CO_2$ data, but the overall decrease in τ_M with x_{CO_2} predicted

in the simulations seems qualitatively sensible. In this regard, it should be noted that Aida and Inomata[19] also simulated the dielectric response of $CH_3OH + CO_2$ mixtures, using different but comparable model potentials. Their simulations, which were performed at 323 K and 11 MPa to enable direct comparison to the Smith experiments, show a complicated composition dependence that is not similar to the smooth behavior reported here. In contrast, the magnitude and composition dependence of ϵ_r reported by Aida and Inomata[19] is similar to ours, so that reason for the difference in dielectric times is unclear.

V. Summary and Conclusions

We have simulated a number of properties of the gas-expanded liquids $c\text{-}C_6H_{12} + CO_2$, $CH_3CN + CO_2$, and $CH_3OH + CO_2$ at various compositions along the experimental bubble point curves at 298 K. Our results suggest that simple intermolecular potentials of the sort used here provide at least semiquantitative models of the properties of GXLs relevant to their use as solvents. The simulations indicate that significant changes to the structure of the liquid and solvent sorting only occur for mole fractions of CO_2 greater than about 0.5. In the $c\text{-}C_6H_{12} + CO_2$ system, the mixing appears to be almost completely random even at $x_{CO_2} > 0.9$. In contrast, in the polar mixture $CH_3CN + CO_2$ and especially in the associated mixture $CH_3OH + CO_2$ pronounced solvent sorting takes place. Despite these structural differences, the CO_2 dependence of many of the thermodynamic and dynamic properties is similar in all three of these GXLs. The few direct comparisons to experiment currently available suggest that if a given property is well reproduced in the pure liquid components, the properties predicted for the mixture should be also be reliable.

Acknowledgment. The authors thank Rigoberto Hernandez and Brian Laird for communicating the results of their GXL simulations prior to publication and Zemin Su for help in the initial stages of these simulations. This research was started with funds provided by a grant from the US National Science Foundation (CHE-0241316).

Supporting Information Available: Graphs showing atom−atom radial distribution functions of selected CH_3CN sites in the $CH_3CN + CO_2$ system and of selected CH_3OH sites in the $CH_3OH + CO_2$ system, behavior of ηD vs x for the liquid and CO_2 components of the GXLs, and total dipole moment autocorrelation functions of $CH_3CN + CO_2$ mixtures and $CH_3OH + CO_2$ mixtures. This material is available free of charge via the Internet at http://pubs.acs.org.

References and Notes

(1) Hallett, J. P.; Kitchens, C. L.; Hernandez, R.; Liotta, C. L.; Eckert, C. A. Exploiting the Anomalous Nanoscale Chemistry of Gas-Expanded Liquids (GXLs). *Acc. Chem. Res.*, in press.

(2) Eckert, C. A.; Liotta, C. L.; Bush, D.; Brown, J. S.; Hallett, J. P. Sustainable Reactions in Tunable Solvents. *J. Phys. Chem. B* **2004**, *108*, 18108−18118.

(3) de la Fuente Badilla, J. C.; Peters, C. J.; de Swaan Arons, J. Volume expansion in relation to the gas-antisolvent process. *J. Supercrit. Fluids* **2000**, *17*, 13−23.

(4) Anand, M.; McLeod, M. C.; Bell, P. W.; Roberts, C. B. Tunable Solvation Effects on the Size-Selective Fractionation of Metal Nanoparticles in CO_2 Gas-Expanded Solvents. *J. Phys. Chem. B* **2005**, *109*, 22852−22859.

(5) Dehghani, F.; Foster, N. R. Dense gas anti-solvent processes for pharmeceutical formulation. *Curr. Opin. Solid State Mater. Sci.* **2003**, *7*, 363−369.

(6) Jung, J.; Perrut, M. Particle Design Using Supercritical Fluids: Literature and Patent Survey. *J. Supercrit. Fluids* **2001**, *20*, 179−219.

(7) Cui, Y.; Olesik, S. V. High-Performance Liquid Chromatography Using Mobile Phases with Enhanced Fluidity. *Anal. Chem.* **1991**, *63*, 1812−1819.

(8) Olesik, S. V. Physicochemical properties of enhanced-fluidity solvents. *J. Chromatogr., A* **2004**, *1037*, 405−410.

(9) Song, I.; Spuller, M.; Levitin, G.; Hess, D. W. Photoresist and Residue Removal Using Gas-Expanded Liquids. *J. Electrochem. Soc.* **2006**, *153*, G314−G318.

(10) Xie, X.; Liotta, C. L.; Eckert, C. A. CO_2−Catalyzed Acetal Formation in CO_2-Expanded Methanol and Ethylene Glycol. *Ind. Eng. Chem. Res.* **2004**, *43*, 2605−2609.

(11) Wei, M.; Musie, G. T.; Busch, D. H.; Subramaniam, B. Autoxidation of 2,6-di-tert-butylphenol with cobalt Schiff base catalysts by oxygen in CO2-expanded liquids. *Green Chem.* **2004**, *6*, 387−393.

(12) Musie, G.; Wei, M.; Subramaniam, B.; Busch, D. H. Catalytic oxidations in carbon dioxide-based reaction media, including novel CO_2-expanded phases. *Coord. Chem. Rev.* **2001**, *219*−*221*, 789−820.

(13) Wyatt, V. T.; Bush, D.; Lu, J.; Hallett, J. P.; Liotta, C. L.; Eckert, C. A. Determination of solvatochromic solvent parameters for the characterization of gas-expanded liquids. *J. Supercrit. Fluids* **2005**, *36*, 16−22.

(14) Chen, J.; Shen, D.; Wu, W.; Han, B.; Sun, D. Solvatochromic behavior of phenol blue in CO2 + ethanol and CO_2 + *n*-pentane mixtures in the critical region and local composition enhancement. *J. Chem. Phys.* **2005**, *122*, 204508.

(15) Sala, S.; Tassaing, T.; Ventosa, N.; Danten, Y.; BEsnard, M.; Veciana, J. Molecular Insight, through IR Spectroscopy, on Solvating Phenomena Occuring in CO_2-Expanded Solutions. *ChemPhysChem* **2004**, *5*, 243−245.

(16) Kelley, S. P.; Lemert, R. M. Solvatochromic Characterization of the Liquid Phase in Liquid-Supercritical CO_2 Mixtures. *AIChE J.* **1996**, *42*, 2047−2056.

(17) Moon, S. D. Monte Carlo simulation for vapor-liquid equilibrium of binary mixtures CO_2/CH_3OH, CO_2/C_2H_5OH, and $CO_2/CH_3CH_2CH_2OH$. *Bull. Korean Chem. Soc.* **2002**, *23*, 811−816.

(18) Chatzis, G.; Samios, J. Binary mixtures of supercritical carbon dioxide with methanol. A molecular dynamics simulation study. *Chem. Phys. Lett.* **2003**, *374*, 187−193.

(19) Aida, T.; Inomata, H. MD Simulation of the Self-Diffusion Coefficient and Dielectric Properties of Expanded Liquids - Methanol and Carbon Dioxide Mixtures, I. *Mol. Simul.* **2004**, *30*, 407−412.

(20) Stubbs, J. M.; Siepmann, J. I. Binary phase behavior and aggregation of dilute methanol in supercritical carbon dioxide: A Monte Carlo simulation study. *J. Chem. Phys.* **2004**, *121*, 1525−1534.

(21) Houndonougbo, Y.; Guo, J.; Lushington, G. H.; Laird, B. Monte Carlo Simulations of CO_2-expanded Acetonitrile. *Mol. Phys.*, in press.

(22) Houndonougbo, Y.; Jin, H.; Rajagopalan, B.; Wong, K.; Kuczera, K.; Subramaniam, B.; Laird, B. Phase Equilibria in Carbon-Dioxide Expanded Solvents: Experiments and Molecular Simulations. *J. Phys. Chem. B* **2006**, *110*, 13195−13202.

(23) Shukla, C. L.; Hallett, J. P.; Popov, A. V.; Hernandez, R.; Liotta, C. L.; Eckert, C. A. Molecular Dynamics Simulation of the Cybotactic Region in Gas-Expanded Methanol-Carobon Dioxide and Acetone-Carbon Dioxide Mixtures. Submitted to *J. Phys. Chem.*

(24) DL_POLY_2, in *Version 2.14*; Smith, W., Forester, T. R., Eds.; CCLRC Daresbury Laboratory: Daresbury, U.K., 2001. The program was modified from the standard version only through incorporation of various routines used to collect data of interest during the course of a simulation rather than by postprocessing saved coordinate data.

(25) Frenkel, D.; Smit, B. *Understanding Molecular Simulation, From Algorithms to Applications*, 2nd ed.; Academic Press: New York, 2002.

(26) Calculation of these quantities was performed using Monte Carlo sampling as described in ref 52.

(27) Marcus, Y.; *Solvent Mixtures, Properties and Selective Solvation*; Marcel-Dekker: New York, 2002.

(28) Hill, T. L. *An Introduction to Statistical Thermodynamics*; Addison-Wesley: Reading, MA, 1960.

(29) Li, H.; Arzhantsev, S.; Maroncelli, M. Solvation & Solvatochromism in CO_2-Expanded Liquids. 2. Experiment − Simulation Comparisons in Three Prototypical Systems. *J. Phys. Chem. B.* Manuscript in preparation.

(30) Hauser, R. A.; Zhao, J. P.; Tremaine, P. R.; Mather, A. E. Excess molar enthalpies of six (carbon dioxide a polar solvent) mixtures at the temperatures 298.15 and 308.15 K and pressures from 7.5 to 12.6 MPa. *J. Chem. Thermodyn.* **1996**, *28*, 1303−1317.

(31) Marcus, Y. *The Properties of Solvents*; Wiley: New York, 1998.

(32) Allen, M. P.; Tildesley, D. J. *Computer Simulation of Liquids*; Oxford University Press: Oxford, 1987.

(33) Because these correlation functions are fairly noisy, we used a combination of numerical integration and fitting to one or two $\cosh^2(at)$ functions in order to determine the required integral values.

(34) Heitz, M. P.; Maroncelli, M. Rotation of Solutes in Supercritical CO_2: Are Rotation Times Anomalously Slow in the Near Critical Regime? *J. Phys. Chem. A* **1997**, *101*, 5852−5868.

(35) Kumar, P. V.; Maroncelli, M. Polar Solvation Dynamics of Polyatomic Solutes: Simulation Studies in Acetonitrile and Methanol. *J. Chem. Phys.* **1995**, *103*, 3038−3060.

(36) Walser, R.; Mark, A.; van Gunsteren, W.; Lauterbach, M.; Wipff, G. The effect of force-field parameters on properties of liquids: Parametrization of a simple three-site model for methanol. *J. Chem. Phys.* **2000**, *112*, 10450−10459.

(37) Khajehpour, M.; Welch, C. M.; Kleiner, K. A.; Kauffman, J. F. Separation of Dielectric Nonideality from Preferential Solvation in Binary Solvent Systems: An Experimental Examination of the Relationship between Solvatochromism and Local Solvent Compostition around a Dipolar Solute. *J. Phys. Chem. A* **2001**, *105*, 5372−5379.

(38) Smith, R. D.; Saito, C.; Suzuki, S.; Lee, S. B.; Inomata, H.; Arai, K. Temperature dependence of dielectric spectra of carbon dioxide and methanol mixtures at high pressures. *Fluid Phase Equilib.* **2002**, *194*−*197*, 869−877.

(39) Harris, J. G.; Yung, K. H. Carbon Dioxide's Liquid−Vapor Coexistence Curve and Critical Properties As Predicted by a Simple Molecular Model. *J. Phys. Chem.* **1995**, *99*, 12021−12024.

(40) Jorgensen, W. L.; Madura, J. D.; Swenson, C. J. Optimized Intermolecular Potential Functions for Liquid Hydrocarbons. *J. Am. Chem. Soc.* **1984**, *106*, 6638−6646.

(41) Edwards, D. M. F.; Madden, P. A.; McDonald, I. R. A Computer Simulation Study of the Dielectric Properties of a Model of Methyl Cyanide: The Rigid Dipole Case, I. *Mol. Phys.* **1984**, *51*, 1141−1161.

(42) Haughney, M.; Ferrario, M.; McDonald, I. R. Molecular-Dynamics Simulation of Liquid Methanol. *J. Phys. Chem.* **1987**, *91*, 4934−4940.

(43) Gray, C. G.; Gubbins, K. E. *Theory of Molecular Fluids*; Oxford University Press: New York, 1984.

(44) These calculations were performed using the SUPERTRAPP program Version 3.1 (NIST Standard Reference Database 4). The calculations employed the Peng−Robinson equation of state with van der Waals one-fluid mixing rules and the binary interaction parameter $k_{ij} = 0.109$. We have found these calculations to provide accurate representations of the relevant properties of the *n*-pentane + CO_2 mixture as well as the pressure−composition data available for the c-C_6H_{12} + CO_2 system.[53]

(45) Kordikowski, A.; Schenk, A. P.; Van Nielsen, R. M.; Peters, C. J. Volume Expansions and Vapor-Liquid Equilibria of Binary Mixtures of a Variety of Polar Solvents in Certain Near-Critical Solvents. *J. Supercrit. Fluids* **1995**, *8*, 205−216.

(46) Brunner, E.; Hueltenschmidt, W.; Schlichthaerle, G. Fluid mixtures at high pressures. IV. Isothermal phase equilibria in binary mixtures consisting of (methanol + hydrogen or nitrogen or methane or carbon monoxide or carbon dioxide). *J. Chem. Thermodyn.* **1987**, *19*, 273−291.

(47) Lemmon, E. W.; McLinden, M. O.; Friend, D. G. Thermophysical Properties of Fluid Systems. In *Standard Reference Database Number 69*; Linstrom, P. J., Mallard, W. G., Eds.; National Institute of Standards and Technology: Gaithersburg, MD, 2005.

(48) Barthel, J.; Bachhuber, K.; Buchner, R.; Hetzenauer, H. Dielectric Specra of Some Common Solvents in the Microwave Region. Water and Lower Alcohols. *Chem. Phys. Lett.* **1990**, *165*, 369−373.

(49) Barthel, J.; Kleebauer, M.; Buchner, R. Dielectric Relaxation of Electrolyte Solutions in Acetonitrile. *J. Solution Chem.* **1995**, *24*, 1−17.

(50) Liu, H.; Macedo, E. A. Accurate Correlations for the Self-Diffusion Coefficients of CO_2, CH_4, C_2H_4, H_2O, and D_2O over Wide Ranges of Temperature and Pressure. *J. Supercrit. Fluids* **1995**, *8*, 310−317.

(51) Lewis, J.; Biswas, R.; Robinson, A.; Maroncelli, M. Local Density Augmentation in Supercritical Fluids: Electronic Shifts of Anthracene Derivatives. *J. Phys. Chem. B* **2001**, *105*, 3306−3318.

(52) Song, W.; Biswas, R.; Maroncelli, M. Intermolecular Interactions and Local Density Augmentation in Supercritical Solvation: A Survey of Simulation and Experimental Results. *J. Phys. Chem. A* **2000**, *104*, 6924−6939.

(53) Kaminishi, G. I.; Yokoyama, C.; Takahashi, S. Vapor pressures of binary mixtures of carbon dioxide with benzene, *n*-hexane and cyclohexane up to 7 MPa. *Fluid Phase Equilib.* **1987**, *34*, 83−99.